Targeted Delivery of a Sialic Acid-Blocking Glycomimetic to Cancer Cells Inhibits Metastatic Spread

Christian Büll,[†] Thomas Jan Boltje,[‡] Eric A. W. van Dinther,[†] Timo Peters,[‡] Annemarie M. A. de Graaf,[†] Jeanette H. W. Leusen,[§] Martin Kreutz,[†] Carl G. Figdor,[†] Martijn H. den Brok,[†] and Gosse J. Adema*[,†]

[†]Department of Tumor Immunology, Radboud Institute for Molecular Life Sciences, Radboud University Medical Center, Geert Grooteplein 28, 6525 GA Nijmegen, The Netherlands, [‡]Cluster for Molecular Chemistry, Institute for Molecules and Materials, Radboud University Nijmegen, Heyendaalseweg 135, 6525 AJ Nijmegen, The Netherlands, and [§]Immunotherapy Laboratory, Laboratory for Translational Immunology, University Medical Center Utrecht, Heidelberglaan 100, 3584 CX Utrecht, The Netherlands

ABSTRACT Sialic acid sugars are overexpressed by cancer cells and contribute to the metastatic cascade at multiple levels. Therapeutic interference of sialic acids, however, has been difficult to pursue because of the absence of dedicated tools. Here we show that a rationally designed sialic acid-blocking glycomimetic (P-3F$_{ax}$-Neu5Ac) successfully prevents cancer metastasis. Formulation of P-3F$_{ax}$-Neu5Ac into poly(lactic-*co*-glycolic acid nanoparticles coated with antityrosinase-related protein-1 antibodies allowed targeted delivery of P-3F$_{ax}$-Neu5Ac into melanoma cells, slow release, and long-term sialic acid blockade. Most importantly, intravenous injections of melanoma-targeting P-3F$_{ax}$-Neu5Ac nanoparticles prevented metastasis formation in a murine lung metastasis model. These findings stress the importance of sialoglycans in cancer metastasis and advocate that sialic acid blockade using rationally designed glycomimetics targeted to cancer cells can effectively prevent cancer metastases. This targeting strategy to interfere with sialic acid-dependent processes is broadly applicable not only for different types of cancer but also in infection and inflammation.

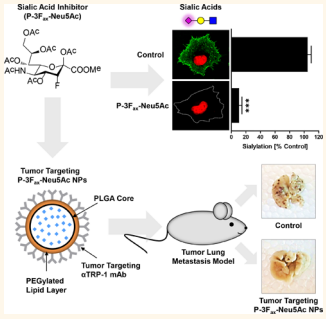

KEYWORDS: sialic acids · glycomimetic · PLGA nanoparticles · cancer · metastasis

Evidence is accumulating that aberrant glycosylation and in particular overexpression of sialic acid sugars by cancer cells are involved in and possibly drive distinct processes during cancer metastasis.[1−7] Dissemination of cancer cells from primary tumors and metastases formation in distant organs is the major cause of cancer-associated mortality.[8,9] Therefore, preventing dissemination of tumor cells and their growth at secondary sites are key to effective cancer therapy. Following successful detachment from the primary tumor, cancer cells can invade the surrounding tissue, enter the circulation *via* blood vessels or lymphatic vessels, form immune protective thromboemboli, extravasate from the circulation, proliferate and form metastases.[10−12] Each of these steps during metastatic spread requires multiple biochemical interactions between different cell types as well as the extracellular matrix (ECM) involving both proteins and carbohydrates.[13] Especially sialic acids that are aberrantly expressed on cancer cells appear to facilitate several steps of the metastatic cascade.[14,15] Sialic acids (Neu5Ac) comprise a diverse family of sugar molecules that terminate glycans (sialoglycans) of cell surface glycoproteins and glycolipids in virtually all vertebrate cells. Sialoglycans are formed in the Golgi system by a family of 20 sialyltransferases. Sialyltransferases specifically conjugate sialic acids to other sugar molecules in glycans *via* distinct glycosidic linkages yielding α2,3-, α2,6- or α2,8-linked sialic acids.[16] Upon malignant transformation, cancer cells upregulate sialyltransferase expression resulting in the accumulation of sialoglycans on their surface.[17,18] Aberrantly high sialic acid expression favors cancer metastasis by (i) facilitating cancer cell detachment and protection from detachment-induced apoptosis (anoikis); (ii) enhancing migration and tissue invasion by increasing integrin interactions with the ECM; (iii) preventing immune recognition and eradication; and (iv) enabling

* Address correspondence to gosse.adema@radboudumc.nl.

Received for review October 30, 2014 and accepted January 9, 2015.

Published online January 09, 2015
10.1021/nn5061964

interactions with endothelial cells to extravasate from the bloodstream and form metastases.[14,15,19−22]

Interference with sialic acid expression in cancer cells could thus be of crucial importance in preventing cancer metastasis as multiple steps of the metastatic cascade could be targeted at the same time. Accordingly, desialylation of cancer cells by overexpressing human sialidases or treatment with bacterial sialidases have been reported to inhibit metastases formation in murine metastasis models.[23−27] However, gene therapy is challenging and bacterial sialidases are difficult to obtain in clinical grade quality. Therefore, synthetic small molecules that inhibit sialic acid expression in cancer cells could be of high therapeutic value. We have recently explored the therapeutic potential of a global sialyltransferase inhibitor P-3F$_{ax}$-Neu5Ac that has been developed by Rillahan *et al.*[28] P-3F$_{ax}$-Neu5Ac is a peracetylated analogue of natural occurring Neu5Ac that due to attachment of a fluorine atom to the sialic acid backbone can inhibit sialyltransferase function and hence sialylation. We previously demonstrated that treatment of murine melanoma cells with this glycomimetic strongly impaired their binding to ECM components and migratory capacity *in vitro*, and delayed tumor growth *in vivo*.[29] Here, we report for the first time that pretreatment of mouse melanoma cells with P-3F$_{ax}$-Neu5Ac to block sialylation prevented lung metastases *in vivo*. Moreover, encapsulation of P-3F$_{ax}$-Neu5Ac in biodegradable poly(lactic-*co*-glycolic acid) (PLGA)-based nanoparticles (NPs) targeting the melanoma antigen tyrosinase-related protein-1 (TRP-1) allowed specific and prolonged blockade of sialic acid expression *in vitro* and precluded metastatic spread *in vivo*.

RESULTS

P-3F$_{ax}$-Neu5Ac Inhibits B16−F10 Lung Metastases Formation. Sialoglycans have been indicated to facilitate multiple steps during cancer metastasis. Previously, we showed that a rationally designed glycomimetic, P-3F$_{ax}$-Neu5Ac, efficiently blocked sialic acid expression in tumor cells and reduced their adhesive and migratory capacity.[29] Therefore, we evaluated the potential of P-3F$_{ax}$-Neu5Ac to inhibit cancer metastasis in an experimental pulmonary metastasis model. Hereto, B16−F10 cells were cultured 3 days in the presence or absence of P-3F$_{ax}$-Neu5Ac (23.1 μg/mL) and expression of cell surface sialic acids was determined by flow cytometry using biotinylated lectins conjugated to streptavidin-phycoerythrin. Expression of α2,3-linked sialic acids was reduced by 90% (Figure 1a), and α2,6-inked sialic acids by 80% (Figure 1b) as detected with the lectins MALII and SNA-I, respectively. Accordingly, binding of the β-galactose-recognizing lectin PNA strongly increased (Figure 1c). Cell viability was not affected by treatment with the glycomimetic (Figure S1a, Supporting Information). Having confirmed blocked sialylation, treated and untreated B16−F10 tumor cells were extensively washed and injected into the tail vein of mice. Fourteen days post injection, mice were sacrificed, lungs were isolated and pulmonary lesions enumerated. Untreated cells on average formed ±50 metastatic nodules in the lung. Treatment with P-3F$_{ax}$-Neu5Ac reduced the number of pulmonary lesions to an average of about 10 nodules (80% reduction) (Figure 1d,e). Treatment with *Clostridium perfringens* sialidase decreased sialic acid levels and metastatic lesions in the lung to a similar extent confirming that the effects are due to removal of sialic acids (Figure S1b,c). Apart from the lung, metastatic lesions were not detected in other organs. These data suggest that sialoglycans are a prerequisite for effective metastasis formation and that P-3F$_{ax}$-Neu5Ac is a potent inhibitor of experimental metastases and therefore interesting to explore in anticancer therapy.

Encapsulation of P-3F$_{ax}$-Neu5Ac into PLGA Nanoparticles. The potent effects of P-3F$_{ax}$-Neu5Ac pretreatment on tumor growth and metastasis prompted us to develop sialic acid blockade for *in vivo* applications. As sialic acids play a vital role in physiology and systemic administration of the glycomimetic could lead to adverse effects,[16] we developed a therapeutic strategy for the specific delivery of this sialic acid-blocking glycomimetic to tumor cells *in vivo*. To this end, we encapsulated P-3F$_{ax}$-Neu5Ac only or in combination with fluorescent ATTO 647 dye into biodegradable, FDA-approved poly(lactic-*co*-glycolic acid) (PLGA)-based nanoparticles that have previously been described by others and our own group.[30−32] The formulated NPs had an average size of about 200 nm (polydispersity index: 0.118 ± 0.063; Zeta potential: −30.4 mV) and contained 23.1 μg P-3F$_{ax}$-Neu5Ac per milligram NP as determined with HPLC. P-3F$_{ax}$-Neu5Ac incorporation efficiency was similar when combined with ATTO 647 (Table S1). To determine the effective dose of P-3F$_{ax}$-Neu5Ac-loaded NPs, B16−F10 cells were cultured for 3 days in medium containing increasing amounts of nanoparticles. Sialic acid expression was reduced in a dose-dependent manner (Figure 2a−c). At a 1 mg/mL dose, the NPs were effective in reducing expression of α2,3-linked sialic acids and α2,6-linked sialic acids to the same extent as 23.1 μg/mL soluble P-3F$_{ax}$-Neu5Ac (Figure 2a,b, Figure S2a−e). Accordingly, increased exposure of terminal β-galactose residues upon incubation with P-3F$_{ax}$-Neu5Ac NPs was detected with PNA lectin (Figure 2c, Figure S2f). Noteworthy, neither P-3F$_{ax}$-Neu5Ac-loaded nor control PLGA NPs affected cell viability and even a concentration of 2 mg/mL empty PLGA nanoparticles did not influence overall cell surface glycosylation (Figure S3). A comparable sialic acid blockade was observed for P-3F$_{ax}$-Neu5Ac NPs co-loaded with the fluorescent ATTO 647 (P-3F$_{ax}$-Neu5Ac/A647 NPs) (Figure S4). Using these fluorescent

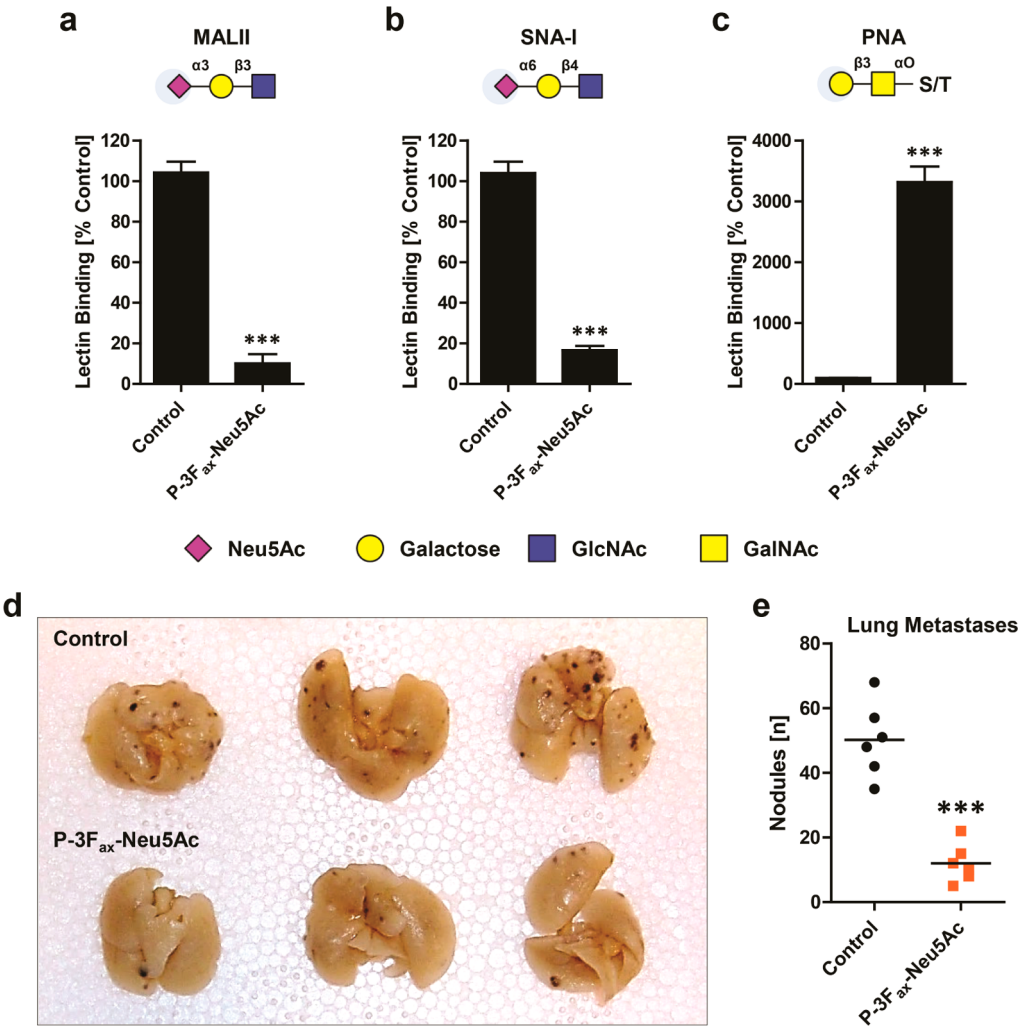

Figure 1. Blocking sialic acid expression using P-3F$_{ax}$-Neu5Ac impairs B16−F10 metastases formation. (a−c) P-3F$_{ax}$-Neu5Ac efficiently blocks sialylation. B16−F10 cells were cultured for 3 days with or without 23.1 μg/mL P-3F$_{ax}$-Neu5Ac and expression of α2,3-linked sialic acids, α2,6-linked sialic acids, and terminal β-galactose was quantified by flow cytometry using biotinylated lectins MALII (a), SNA-I (b) or PNA (c) conjugated to streptavidin-PE. Fluorescence values were normalized to untreated control cells and data of three independent experiments are presented as average percentage lectin binding ± SEM. (d,e) Metastases formation of B16−F10 cells incubated 3 days with or without 23.1 μg/mL P-3F$_{ax}$-Neu5Ac. Prior to injection, cells were washed extensively and 0.5 × 10^6 cells were injected into the tail vein of mice (n = 6). Fourteen days later, mice were sacrificed and lungs were collected and fixed overnight in Fekete's solution. Representative images of pulmonary lesions are shown (d) and nodules were enumerated and presented in a scatter plot (e).

P-3F$_{ax}$-Neu5Ac/A647 NPs, cellular uptake was readily observed in B16−F10 cells (Figure 2d). Orthogonal projections confirmed that these fluorescent P-3F$_{ax}$-Neu5Ac/A647 NPs were readily taken up into the cytoplasm, most likely the endosomal compartment, of B16−F10 cells (Figure 2d−h).[33,34] Flow cytometry analysis of the P-3F$_{ax}$-Neu5Ac/A647 NPs uptake kinetics showed that already after 1 h a fluorescent signal could be measured in all cells. Signal intensity increased over time reaching a maximum between 8 and 24 h incubation (Figure 2i, Figure S5). Incubation at 4 °C prevented cellular uptake indicating that the NPs are actively taken up and do not adhere to the cell membrane. To demonstrate intracellular degradation, NPs were coloaded with double-quenched (DQ)-BSA that emits fluorescence upon protease cleavage. Following 0.5 to 24 h incubation, increasing fluorescence from cells cultured with DQ-BSA-loaded NPs was detected by flow cytometry (Figure 2j). Furthermore, while incubation with soluble P-3F$_{ax}$-Neu5Ac reduced sialic acid expression upon 1 day of incubation, NP-encapsulated P-3F$_{ax}$-Neu5Ac reduced sialic acid expression after 2 to 3 days incubation (Figure S6). These data indicate that PLGA NPs form neutral carriers that can be effectively loaded with the P-3F$_{ax}$-Neu5Ac glycomimetic to induce sialic acid blockade in tumor cells.

Targeted Delivery of P-3F$_{ax}$-Neu5Ac-Containing Nanoparticles to B16−F10 Cells. B16−F10 cells express the melanoma associated antigen tyrosinase-related protein-1 (TRP-1) that is involved in melanin synthesis on their surface (Figure 3a, Figure S7a).[35] TRP-1 has been shown to

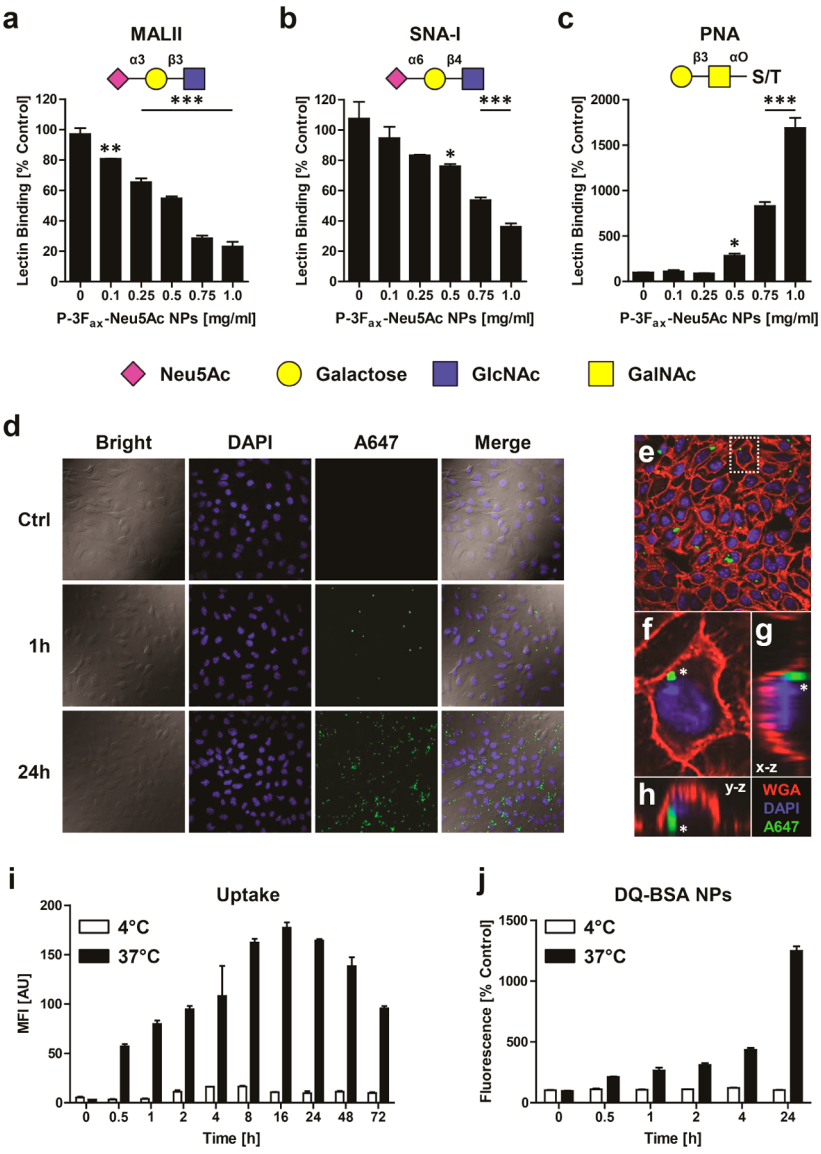

Figure 2. P-3F$_{ax}$-Neu5Ac NPs block sialylation and are readily taken up and degraded by B16−F10 cells. (a−c) B16−F10 cells were cultured for 3 days with 0−1 mg/mL P-3F$_{ax}$-Neu5Ac NPs and expression of α2,3-linked sialic acids, α2,6-linked sialic acids, and terminal β-galactose was quantified by flow cytometry using biotinylated lectins MALII (a), SNA-I (b) or PNA (c) conjugated to streptavidin-PE. Fluorescence values were normalized to untreated control cells presented as average percentage lectin binding ± SEM. (d−h) B16−F10 cells were cultured on glass slides in the presence of 1 mg/mL P-3F$_{ax}$-Neu5Ac/A647 NPs. Representative confocal images show cell outlines (bright), nuclei (blue) and ATTO 647 fluorescence (green) following 1 or 24 h culture (d). Following 2 h incubation with P-3F$_{ax}$-Neu5Ac/A647 NPs, B16−F10 cells were stained with DAPI (blue) and biotinylated WGA-NeutrAvidin-Texas Red conjugates (red) to visualize the cell membrane. A representative overview image (e), magnification of a selected cell (stepped lines) (f) and reconstructed orthogonal projections as viewed in the xz-plane (g) and yz-plane (h) show intracellular localization of P-3F$_{ax}$-Neu5Ac/A647 NPs (green). (i) Uptake of P-3F$_{ax}$-Neu5Ac/A647 NPs in B16−F10 cells cultured 0−72 h at 4 or 37 °C was quantified using flow cytometry. Mean fluorescence intensity values of three independent experiments ± SEM are presented. (j) B16−F10 cells were incubated for 0−24 h at 4 or 37 °C with 1 mg/mL nanoparticles containing double-quenched bovine serum albumin (DQ-BSA). Sixteen hours after removal of the NPs from medium, degradation of NPs and DQ-BSA was measured by flow cytometry. Percentage fluorescence normalized to control of three independent experiments ± SEM is shown.

rapidly internalize at the surface,[36] and was therefore chosen to deliver P-3F$_{ax}$-Neu5Ac nanoparticles specifically to B16−F10 cells. To this aim, P-3F$_{ax}$-Neu5Ac or P-3F$_{ax}$-Neu5Ac/A647 nanoparticles were coated with a lipid PEG layer and monoclonal anti-TRP-1 (clone TA99) or isotype control (IgG2a κ) antibodies (Figure 3b). Flow cytometry analysis confirmed efficient and equal coupling of anti-TRP-1 or isotype control antibodies to NPs as well as equal fluorescence intensities of P-3F$_{ax}$-Neu5Ac/A647 NPs (Figure 3c, Figure S7b). Confocal microscopy analysis of the binding of the antibody-conjugated nanoparticles to B16−F10 cells demonstrated that almost no fluorescent signal could be detected at the surface of cells incubated with isotype control antibody-coated P-3F$_{ax}$-Neu5Ac/A647 NPs (Figure 3d). In contrast, TRP-1-targeting NPs were

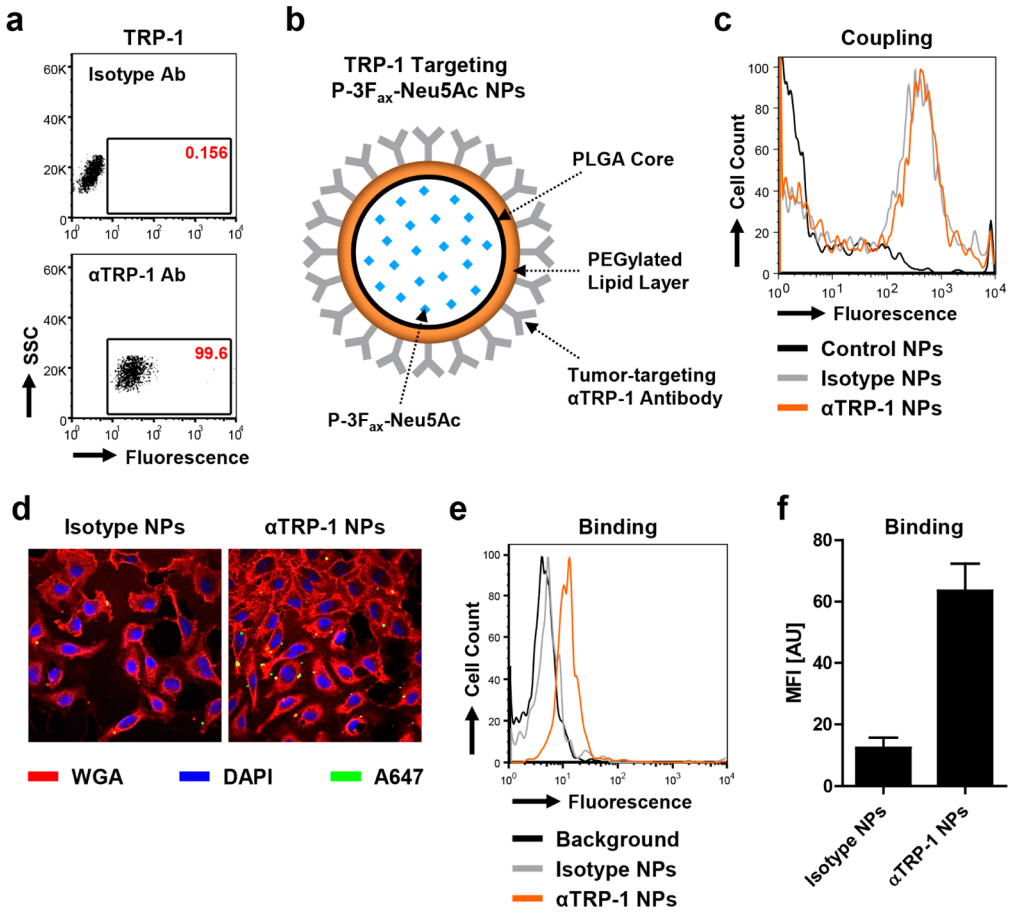

Figure 3. Anti-TRP-1 antibody conjugation allows targeting of P-3F$_{ax}$-Neu5Ac NPs to B16−F10 cells. (a) Representative flow cytometry histograms showing expression of TRP-1 on B16−F10 cells upon staining with anti-TRP-1 antibody (TA99). (b) Structural representation of TRP-1-targeting P-3Fax-Neu5Ac NPs. The glycomimetic was encapsulated in PLGA based nanoparticles with a diameter of 200 nm. The NPs were PEGylated to reduce nonspecific uptake and coated with monoclonal antibodies directed against the melanoma antigen TRP-1. (c) Detection of isotype control or anti-TRP-1 antibody on the surface of P-3F$_{ax}$-Neu5Ac/A647 NPs stained with PE-conjugated antimouse IgG antibody by flow cytometry. (d−f) Binding of anti-TRP-1 P-3F$_{ax}$-Neu5Ac NPs to B16−F10 cells. Confocal images showing binding of isotype control (left) or anti-TRP-1 (right) P-3F$_{ax}$-Neu5Ac/A647 NPs (green) to B16−F10 cells following 15 min incubation at 4 °C (d). Cell membrane was stained with WGA-NeutrAvidin-Texas Red conjugates (red) and nuclei with DAPI (blue). Representative histogram showing fluorescence of B16−F10 cell surface bound isotype control or anti-TRP-1 P-3F$_{ax}$-Neu5Ac/A647 NPs by flow cytometry following 15 min incubation at 4 °C (e). Mean fluorescence intensities ± SEM of B16−F10 cell surface-bound isotype control or anti-TRP-1 P-3F$_{ax}$-Neu5Ac/A647 NPs of three independent experiments determined by flow cytometry (f).

found to bind effectively to the membrane of B16−F10 cells. Subsequent, analysis of the cells with flow cytometry confirmed binding of anti-TRP-1 P-3F$_{ax}$-Neu5Ac/A647 NPs to B16−F10 cells, while isotype control NPs could not bind (Figure 3e,f).

Having confirmed the binding of TRP-1-targeting P-3F$_{ax}$-Neu5Ac NPs to B16−F10 cells, we next assessed uptake and degradation characteristics of these tumor-targeting NPs. Isotype control NPs showed low uptake levels similar to PEGylated control NPs. In contrast, anti-TRP-1 NPs were taken up efficiently by B16−F10 cells (Figure 4a,b). The difference in uptake of isotype control and anti-TRP-1 NPs was confirmed by confocal microscopy (Figure 4c). Intracellular uptake and degradation of TRP-1 antibody-coated NPs, was assessed by coencapsulating DQ-BSA into the NPs. At 1 and 24 h of incubation, fluorescence was markedly higher in B16−F10 cells incubated with anti-TRP-1 DQ-BSA NPs compared to isotype control NPs (Figure 4d). These data indicate that anti-TRP-1 NPs, but not nontargeting isotype control NPs are readily taken up and degraded by B16−F10 cells. Uptake specificity of the anti-TRP-1 NPs was further confirmed by the ability of TRP-1 antibody, but not by isotype control antibody, to block uptake of TRP-1-targeting NPs (Figure 4e,f). In line with these findings, 9464D neuroblastoma cells, which do not express TRP-1, showed similar uptake levels for isotype control and anti-TRP-1 NPs (Figure S7c,d). These data indicate that anti-TRP-1 NPs effectively and specifically are taken up by B16−F10 cells in allowing targeted intracellular delivery of P-3F$_{ax}$-Neu5Ac.

Targeted Delivery of P-3F$_{ax}$-Neu5Ac to B16−F10 and Sustained Sialic Acid Blockade. Having shown specific binding and uptake of anti-TRP-1-targeting NPs, we next investigated the release kinetics of anti-TRP-1-targeting

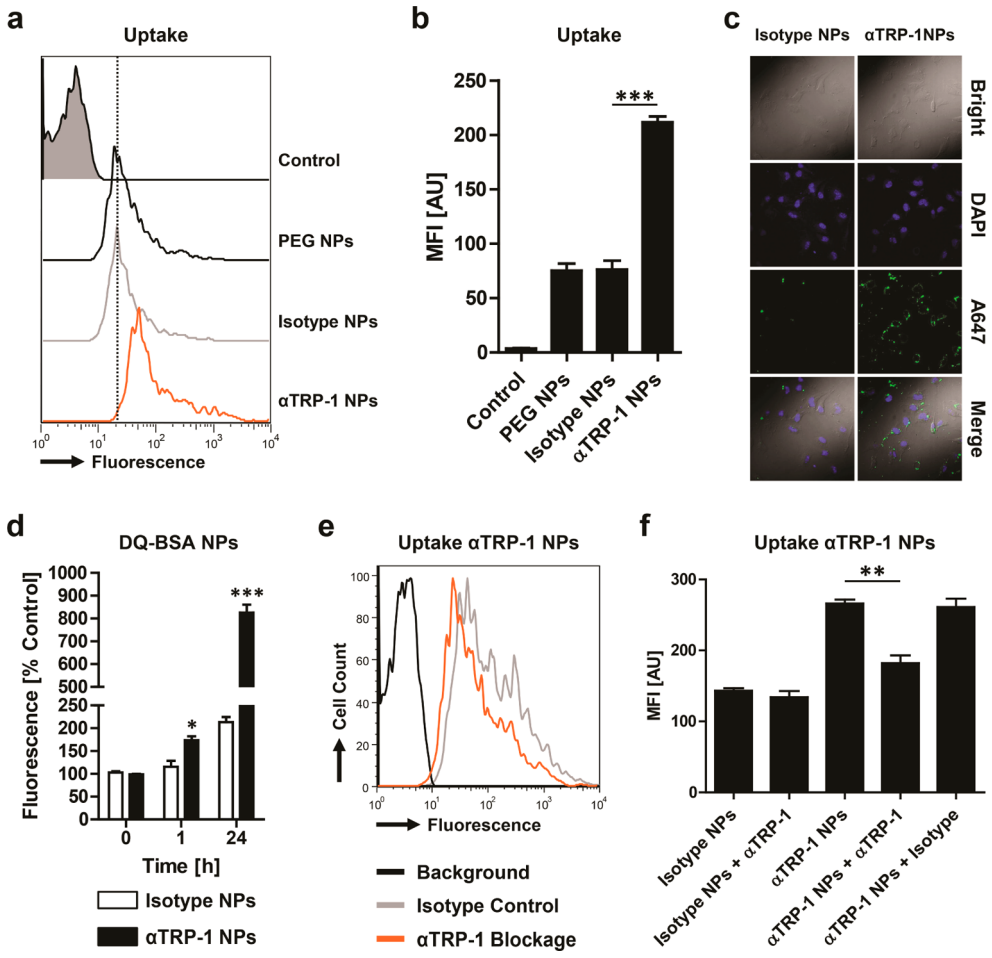

Figure 4. TRP-1-dependent uptake of anti-TRP-1 P-3F$_{ax}$-Neu5Ac NPs in B16−F10 cells. (a−c) Uptake of PEGylated, isotype control antibody- or anti-TRP-1 antibody-coated P-3F$_{ax}$-Neu5Ac/A647 NPs (1 mg/mL) in B16−F10 cells following 16 h incubation at 37 °C. Representative histogram (a) and mean fluorescence intensities ± SEM of three independent experiments (b) showing nanoparticle uptake as determined by flow cytometry. Confocal images of B16−F10 cells following 16 h incubation with isotype control antibody- or anti-TRP-1 antibody-coated P-3F$_{ax}$-Neu5Ac/A647 NPs (green) (c). (d) Uptake and degradation of isotype control antibody- or anti-TRP-1 antibody-coated NPs containing DQ-BSA. B16−F10 cells were incubated with 1 mg/mL nanoparticles for 1 or 24 h and another 16 h later, fluorescence of DQ-BSA was quantified by flow cytometry. Percentage fluorescence normalized to control of three independent experiments ± SEM is shown. (e,f) TRP-1-dependent uptake of anti-TRP-1 antibody-coated P-3F$_{ax}$-Neu5Ac/A647 NPs. B16−F10 cells were preincubated with 10 μg/mL free isotype IgG2a or anti-TRP-1 antibody (TA99) for 20 min, followed by 1 mg/mL isotype IgG2a antibody- or anti-TRP-1 antibody-coated P-3F$_{ax}$-Neu5Ac/A647 NPs for 16 h. Representative histogram showing reduced uptake of anti-TRP-1 NPs upon blockade with anti-TRP-1 antibody (e) and mean fluorescence intensities ± SEM of three independent experiments (f).

NPs containing P-3F$_{ax}$-Neu5Ac. Therefore, B16−F10 cells were incubated for 3 days in the presence of P-3F$_{ax}$-Neu5Ac-loaded isotype control NPs or anti-TRP-1 NPs or with an equal amount of soluble glycomimetic and cell surface sialylation was assessed by lectin binding. Soluble P-3F$_{ax}$-Neu5Ac blocked expression of cell surface sialoglycans potently (Figure 5a−c). In line with the findings that anti-TRP-1 NPs were taken up at high levels compared to isotype control NPs, only anti-TRP-1 P-3F$_{ax}$-Neu5Ac NPs strongly blocked sialylation (80% α2,3-Neu5Ac; 60% α2,6-Neu5Ac) while isotype P-3F$_{ax}$-Neu5Ac NPs only mildly reduced sialic acid expression (40% α2,3-Neu5Ac; 20% α2,6-Neu5Ac). Noteworthy, sialic acid blockade by NP-entrapped P-3F$_{ax}$-Neu5Ac was not due to leakage of the glycomimetic from the NPs, as the NPs remained highly stable in medium for more than 10 days (Figure S8). Following removal of soluble glycomimetic or nanoparticles from culture, recovery of cell surface sialic acid expression was followed in time by flow cytometry using fluorescent lectins. Comparable to unmodified P-3F$_{ax}$-Neu5Ac NPs, anti-TRP-1 P-3F$_{ax}$-Neu5Ac NPs blocked sialylation significantly longer than equal amounts of soluble glycomimetic. α2,3-sialylation was reduced for 6 days, α2,6-sialylation and exposure of terminal β-galactose for 5 days (Figure 5d−f). The mild reduction in sialylation following incubation with isotype control P-3F$_{ax}$-Neu5Ac NPs was restored within 24 h. Altogether, these findings indicate that anti-TRP-1 NPs specifically deliver P-3F$_{ax}$-Neu5Ac to B16−F10 cells and block sialylation for a prolonged period of time due to slow release.

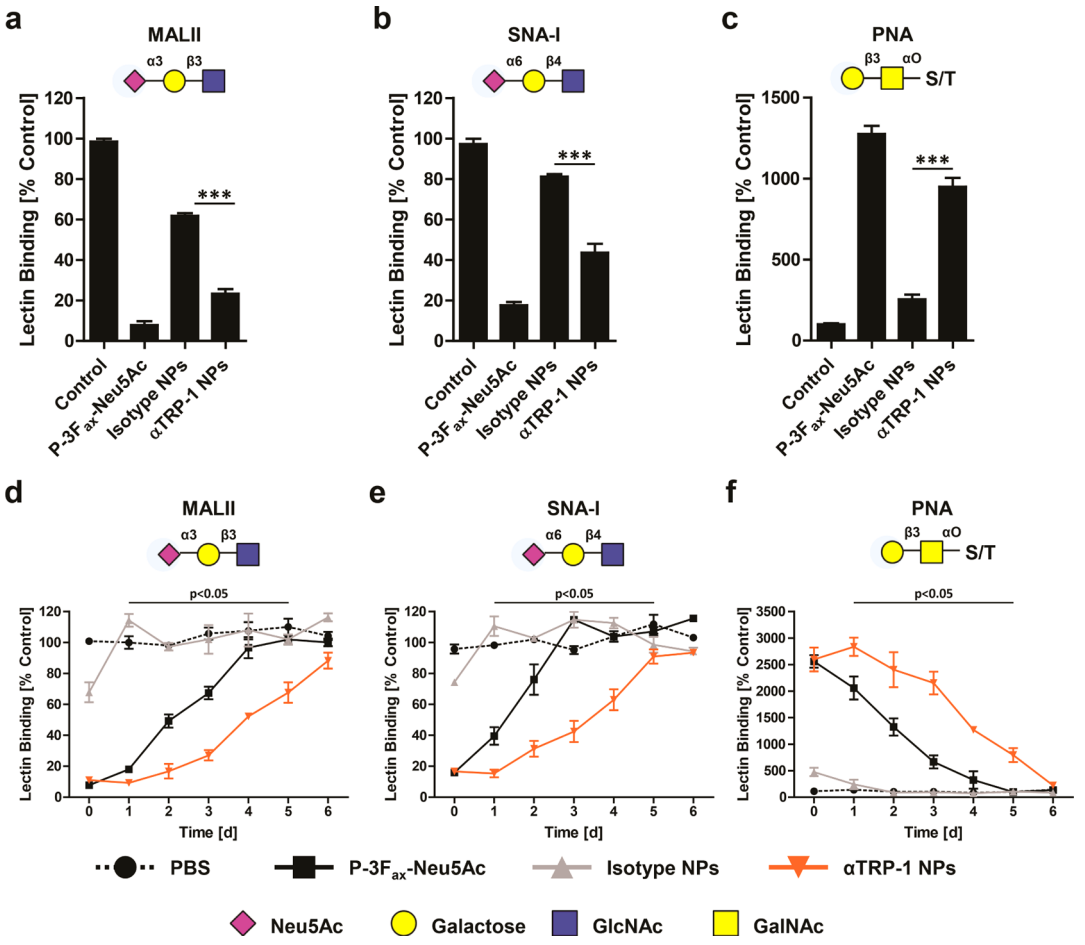

Figure 5. Targeted delivery of P-3F$_{ax}$-Neu5Ac to melanoma and sustained sialic acid blockade. (a–c) B16–F10 cells were cultured for 3 days in the presence of 1 mg/mL isotype control antibody- or anti-TRP-1 antibody-coated P-3F$_{ax}$-Neu5Ac NPs or an equal amount of soluble P-3F$_{ax}$-Neu5Ac (23.1 μg/mL). Expression of α2,3-linked sialic acids, α2,6-linked sialic acids, and terminal β-galactose was quantified by flow cytometry using biotinylated lectins MALII (a), SNA-I (b) or PNA (c) conjugated to streptavidin-PE. (d–f) Recovery of sialylation in time following treatment of B16–F10 cells for 3 days with 1 mg/mL isotype control antibody- or anti-TRP-1 antibody-coated P-3F$_{ax}$-Neu5Ac NPs or an equal amount of soluble P-3F$_{ax}$-Neu5Ac (23.1 μg/mL). Sialic acid expression was measured at several time points by flow cytometry using streptavidin-PE conjugated MALII (d), SNA-I (e) or PNA (f). All fluorescence values were normalized to untreated control cells, and data of three independent experiments are presented as average percentage lectin binding ± SEM.

Targeted Delivery of P-3F$_{ax}$-Neu5Ac Using Anti-TRP-1 NPs Precludes Metastatic Spread *In Vivo*. TRP-1-targeting NPs allowed specific delivery of P-3F$_{ax}$-Neu5Ac to B16–F10 cells and prolonged blockade of sialylation. As *in vitro* pretreatment with the glycomimetic effectively prevented the formation of pulmonary metastases (Figure 1d,e), we now assessed if *in vivo* administration of anti-TRP-1 P-3F$_{ax}$-Neu5Ac NPs could affect metastatic spread *in vivo* (Figure 6a) Following a schedule resembling adjuvant therapy,[37] mice were injected twice intravenously (i.v.) with 20 mg/kg (0.4 mg/mouse) PBS, empty anti-TRP-1 coated NPs, isotype control P-3F$_{ax}$-Neu5Ac NPs or anti-TRP-1 P-3F$_{ax}$-Neu5Ac NPs. One hour after the first injection, 0.5 × 10^6 B16–F10 cells were injected i.v. followed by a second injection with NPs or controls 16 hours after start of the experiment. After 14 days following injection, lungs were isolated and metastatic lesions were enumerated. PBS treated mice showed an average of about ±80 nodules/lung, and administration of empty anti-TRP-1 NPs or P-3F$_{ax}$-Neu5Ac-containing isotype control NPs had no significant impact on the number of nodules (Figure 6b,c). Strikingly, treatment with P-3F$_{ax}$-Neu5Ac-loaded anti-TRP-1 NPs strongly reduced the metastatic load to ±20 nodules/lung (75% reduction). TRP-1 is involved in melanogenesis and B16–F10 cells are known to form both melanin-containing melanotic (black) and amelanotic (gray/white) nodules with low amounts of melanin.[38] Histological analysis of the lungs of the mice treated with anti-TRP-1 P-3F$_{ax}$-Neu5Ac NPs revealed that the detectable metastases essentially lacked melanin (Figure 6d). Additional analysis showed that the number of amelanotic nodules was similar among all treatment groups, but the number of melanotic nodules was decreased by 95% in mice treated with anti-TRP-1 P-3F$_{ax}$-Neu5Ac NPs (Figure 6e). Altogether, these findings demonstrate that sialic acid blockade

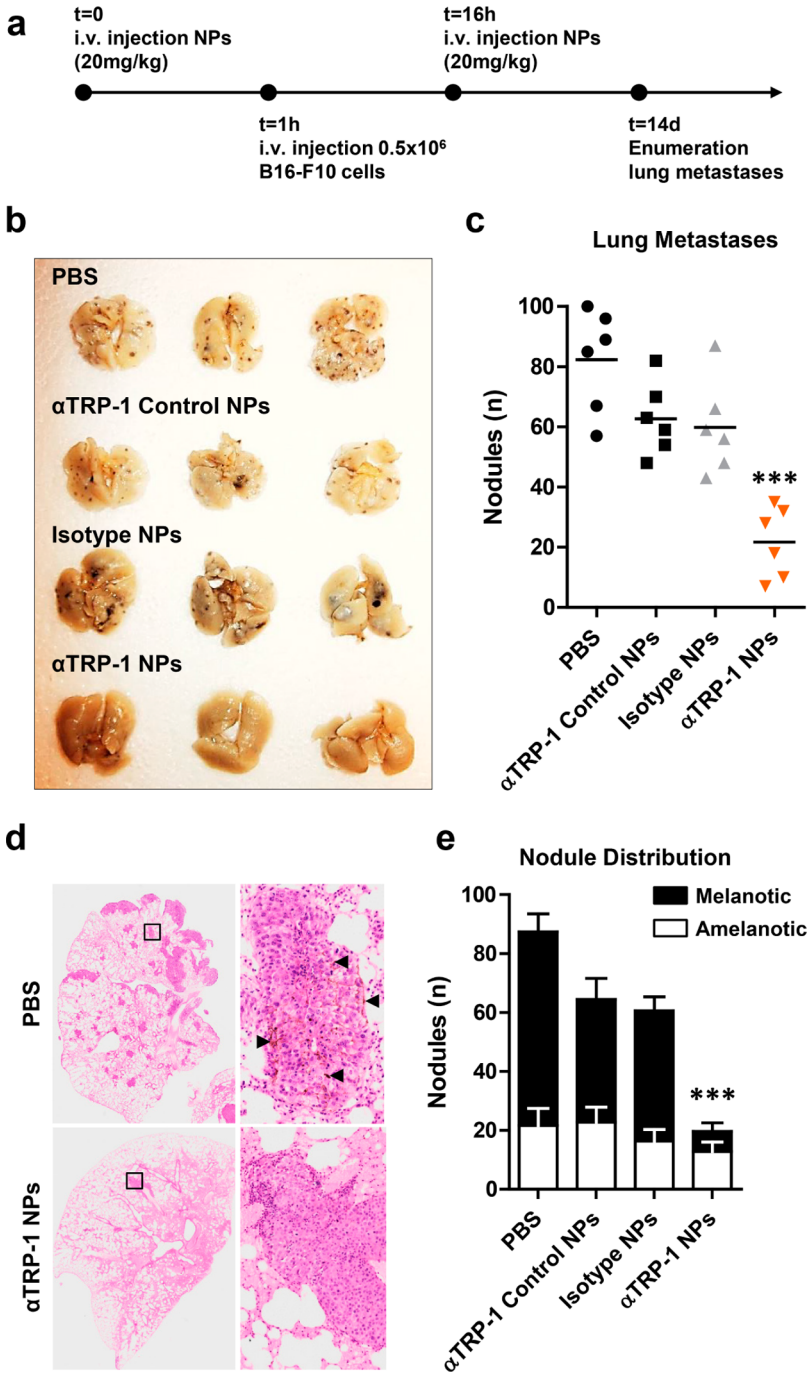

Figure 6. Targeted delivery of P-3F$_{ax}$-Neu5Ac precludes metastatic spread. (a) Treatment schedule. 20 mg/kg isotype control antibody- or anti-TRP-1 antibody-coated P-3F$_{ax}$-Neu5Ac NPs or empty anti-TRP-1 antibody-coated NPs were injected intravenously into the tail vein of mice. One hour later, 0.5 × 10^6 B16−F10 cells were injected into the tail vein of mice (n = 6). Sixteen hours following injection with B16−F10 cells, another dose of 20 mg/kg NPs was administered intravenously, and 14 days later, mice were sacrificed and lungs were collected and fixed overnight in Fekete's solution. Representative images show formation of B16−F10 nodules in the lung (b). All nodules were enumerated and are presented in a scatter dot plot (c). (d) Hematoxylin and eosin staining of lung sections from control or anti-TRP-1 P-3F$_{ax}$-Neu5Ac NPs treated mice. Magnification (squares) shows presence of melanin (arrow) in the metastases of control mice, but not anti-TRP-1 P-3F$_{ax}$-Neu5Ac NPs treated mice. (e) Distribution of melanotic (black) and amelanotic (gray/white) nodules between the treatment groups.

using targeted delivery of P-3F$_{ax}$-Neu5Ac to B16−F10 cells in the bloodstream using anti-TRP-1 NPs largely prevents outgrowth of melanoma cells at distant sites.

DISCUSSION

In this study, we have explored for the first time the possibility to prevent metastases formation by blocking sialic acid expression in cancer cells using a

rationally designed glycomimetic encapsulated into tumor-targeting nanoparticles. In particular we demonstrated that (1) the overexpression of sialic acids may play a role in melanoma cell metastasis, (2) TRP-1 mAb targeted delivery of the sialic acid-blocking glycomimetic P-3F$_{ax}$-Neu5Ac using PLGA nanoparticles allows for long-lasting sialic acid blockade in melanoma cells *in vitro*, (3) therapy with anti-TRP-1 P-3F$_{ax}$-Neu5Ac NPs can prevent metastatic spread of melanoma cells *in vivo*.

Over four decades ago specific tumor characteristics were ascribed to the increased expression of sialic acid sugars on the surface of cancer cells, including effects on tumor growth, escape from apoptosis, metastasis formation and resistance to therapy. Strategies to target aberrant sialylation in cancer, however, have been lacking for a long time. We have recently reported that sialic acid blockade with the broad sialic acid inhibitor P-3F$_{ax}$-Neu5Ac developed by Rillahan and colleagues impaired tumor cell binding to ECM components, migration and tumor cell engraftment.[28,29] Elevated high expression of sialyltransferases and consequently of many different sialoglycans such as the sialyl Lewis x antigen (sLe^x) or α2,6-sialylated integrins have been reported to correlate with aggressiveness of tumors and their ability to form metastases.[1,2,5,14] We now show that pretreatment of B16−F10 cells with soluble glycomimetic remarkably reduced formation of pulmonary metastasis. We have previously reported that P-3F$_{ax}$-Neu5Ac is not toxic for B16−F10 cells nor does affect their proliferation *in vitro* even upon 30 days of culture in the permanent presence of the glycomimetic.[29] Also pretreatment with sialidase reduced the metastatic load to a similar extent. These findings advocate that the reduced metastatic spread is directly related to the blocked sialic acid expression rather than indirect effects of P-3F$_{ax}$-Neu5Ac. The observed potency of sialic acid blockade to prevent cancer metastasis is most likely related to the involvement of sialic acids in many different steps of the metastatic cascade. In our experimental metastasis model, tumor cells possibly are trapped in the bloodstream, because they lack expression of the selectin ligands sLe^x and other sialoglycans that are essential to adhere to selectins on endothelial cells and leave the bloodstream.[4,39] In addition, tumor cells might be cleared from the blood by the immune system because they fail to form immunoprotective thromboemboli with platelets and leukocytes.[6] Furthermore, sialic acid blockade is likely to prevent settlement and growth of the cancer cells in the lung tissue. Indeed, it has been reported that for instance sialoglycans on integrins enable binding to ECM components, provide survival and growth signals, and prevent galectin-induced apoptosis.[40,41] It will be intriguing to unravel how sialic acid blockade exactly prevents metastases formation and which of the steps in the metastasis process depend most on sialic acids.

The potent effects of P-3F$_{ax}$-Neu5Ac pretreatment on tumor growth and metastasis led us to design a therapeutic strategy to deliver this sialic acid-blocking glycomimetic specifically to tumor cells *in vivo* while limiting exposure to normal cells. Nontargeted sialic acid blockade could cause adverse effects as it has been described for mice with defective sialic acid synthesis.[42,43] Therefore, the melanoma specific antigen TRP-1 was selected for the targeting of P-3F$_{ax}$-Neu5Ac loaded PLGA NPs to melanoma tumor cells *in vivo*. Our data showed that TRP-1 mAb targeted delivery of the sialic acid-blocking glycomimetic P-3F$_{ax}$-Neu5Ac using PLGA nanoparticles allowed efficient sialic acid blockade in melanoma cells *in vitro*. TRP-1 itself is a glycoprotein containing complex N-glycans including sialic acids.[44] Sialic acids can influence stability and membrane trafficking and turnover of proteins.[16,45] Interestingly, sialic acid blockade slightly increased expression of TRP-1 and NP uptake, suggesting that delivery of P-3F$_{ax}$-Neu5Ac to B16−F10 cells favors further uptake of anti-TRP-1-coated PLGA NPs (Figure S9). Furthermore, other nanoparticle formulations (*e.g.*, liposomes or micelles) might allow for potent delivery of this sialic acid-blocking glycomimetic to cancer cells.

Disseminated cancer cells circulate in the bloodstream and can form metastases at distant sites.[8,46,47] In several conditions related to the treatment of the primary tumors, like surgery, the number of circulating tumor cells may be enhanced.[48−51] Targeting circulating cancer cells in such conditions may prevent their outgrowth at distant sites and significantly improve the outcome of cancer therapy.[52,53] Using the B16−F10 metastasis model, we now show that anti-TRP-1 NP-mediated targeting of P-3F$_{ax}$-Neu5Ac to these melanoma cells in the circulation prevents their metastatic spread. We are aware that the used anti-TRP-1 antibody alone has antimetastatic effects and is effective for the usage in cancer therapy.[54−56] However, the Fc part of the TRP-1 antibodies conjugated to the PEG lipid layer on NPs might not be available for binding to Fc receptors thereby avoiding antibody-mediated antitumor effects. Indeed, injection of empty anti-TRP-1 conjugated nanoparticles did not significantly affect metastases formation. In contrast, the formation of melanotic nodules was strongly reduced upon injections with anti-TRP-1 NP containing P-3F$_{ax}$-Neu5Ac. The presence of TRP-1, however, is essential as isotype mAb conjugated NPs containing P-3F$_{ax}$-Neu5Ac had no effect. The finding that melanotic but not amelanotic metastases that are known to down-regulate the TRP-1 antigen were reduced provides further evidence that targeting TRP-1 on tumor cells is indeed essential for the observed effects.[57] These data further indicate that targeting multiple different

tumor antigens with P-3F$_{ax}$-Neu5Ac-loaded NPs may be important to counteract antigen escape variants. Finally, no adverse effects or abnormalities at the organ level were found in mice following the injection of two doses of P-3F$_{ax}$-Neu5Ac-loaded NPs, ascribing the treatment a good safety profile. The precise biodistribution and uptake of anti-TRP-1 P-3F$_{ax}$-Neu5Ac NPs *in vivo* as well as alternative treatment schedules and their effect on primary tumor growth remain to be investigated.[58] A small percentage of the anti-TRP-1 P-3F$_{ax}$-Neu5Ac NPs might be taken up by other cell types *in vivo*, as it has been shown for other antibody-nanoparticle conjugates.[59,60] Nevertheless, the striking effects observed *in vivo* provide first evidence that anti-TRP-1 P-3F$_{ax}$-Neu5Ac NPs eventually enrich in melanoma cells.

CONCLUSIONS

In conclusion, our data stress that sialoglycans are essential for cancer metastasis and that rationally designed sialic acid blocking glycomimetics encapsulated in nanoparticles allow specific and safe targeting to tumor cells to prevent metastatic spread. This combined glycobiological and nanotechnological strategy to block sialoglycan expression in specific target cells in blood will be broadly applicable to interfere with sialic acid-dependent processes in cancer, infection and inflammation.

METHODS

Mice. Female C57BL/6J mice were obtained from Harlan Laboratories and housed in the Central Animal Laboratory, Radboud University, Nijmegen, The Netherlands, under specific pathogen-free conditions and *ad libitum* access to food and water. Mice were 6 to 8 weeks old at the beginning of each experiment. All experiments were authorized by the local animal ethics committee, Nijmegen, The Netherlands, and carried out in accordance with their guidelines.

Reagents and Antibodies. P-3F$_{ax}$-Neu5Ac was synthesized as described before.[28,29] PLGA (RG 502 H, Poly(D,L-lactide-*co*-glycolide) 50:50) was purchased from Evonik Industries AG (Essen, Germany), ATTO 647-COOH from ATTO-TEC (Siegen, Germany), DSPE-PEG(2000) Succinyl (1,2-distearoyl-*sn*-glycero-3-phosphoethanolamine-*N*-[succinyl(polyethylene glycol)-2000] (ammonium salt)) and 14:0 PEG2000 PE.

1,2-Dimyristoyl-*sn*-glycero-3-phosphoethanolamine-*N*-[methoxy(polyethylene glycol)-2000] (ammonium salt) from Avanti Polar Lipids, Inc. (Alabaster, AL), Biotinylated lectins MALII (*Maackia amurensis*), SNA-I (*Sambucus nigra*) and carbo-free blocking solution from Vector Laboratories, Inc. (Burlingame, CA). Biotinylated PNA (*Arachis hypogaea*) and WGA (*Triticum vulgaris*) was purchased from EY Laboratories Inc. (San Mateo, CA), 7-AAD viability dye and purified isotype IgG2a κ antibody from eBioscience (San Diego, CA), streptavidin-phycoerythrin and phycoerythrin conjugated goat antimouse IgG from BD Pharmingen (Franklin Lakes, NJ), NeutrAvidin-Texas Red, DAPI nucleic acid stain, Alexa Fluor 647 conjugated goat antimouse IgG (H+L) antibody and double-quenched green bovine serum albumin (DQ-BSA) from Molecular Probes, Inc. (Eugene, OR) and Mowiol 4−88 mounting medium from Merck (Frankfurt, Germany). Mouse anti-TRP-1 antibody (clone TA99, IgG2a κ) was purified from hybridoma cell line HB-8704 (ATCC, Manassas, VA) as previously described.[56]

Nanoparticle Synthesis and Antibody Conjugation. PLGA nanoparticles with entrapped P-3F$_{ax}$-Neu5Ac alone or in combination with ATTO 647-COOH were prepared using an o/w emulsion and solvent evaporation−extraction method as was described before.[31] Briefly, 25 mg of PLGA in 750 μL of dichloromethane containing P-3F$_{ax}$-Neu5Ac (200 mg in 200 μL of DMSO) and ATTO 647-COOH (0.25 mg in 12.5 μL of DMSO) was added dropwise to 6.25 mL of aqueous 2% poly(vinyl alcohol) and emulsified for 120 s using a digital sonicator from Branson Ultrasonics (Danbury, CT). The solvent was evaporated overnight at 4 °C and nanoparticles were collected by centrifugation at 14 000 rpm for 20 min, washed six times with distilled water and lyophilized. Nanoparticles were coated with DSPE-PEG(2000) succinyl and 14:0 PEG2000 PE in a 1:1 ratio and conjugated with mouse anti-TRP-1 or isotype control IgG2a κ antibodies as described previously.[31] Presence of anti-TRP-1 or isotype control antibodies on the particle surface was confirmed by staining nanoparticles with phycoerythrin-conjugated goat antimouse IgG antibodies. Fluorescence was measured using a CyAn ADP flow cytometer (Beckman Coulter, Brea, CA) and quantified utilizing FlowJo software (Tree Star, Ashland, OR)

Nanoparticle Characterization. Size, polydispersity index and zeta potential of the nanoparticles was analyzed by dynamic light scattering using a Zetasizer Nano ZS (Malvern Instruments Ltd., Malvern, UK) as described before.[31] Concentration of P-3F$_{ax}$-Neu5Ac in nanoparticles was determined using a high-performance liquid chromatography (HPLC) system (Shimadzu, Kyoto, Japan) equipped with a Supelcosil lC-18-T column (150 mm × 4.6 mm) with a constant flow rate of 1 mL/min and ultraviolet detection at a wavelength of 230 nm. P-3F$_{ax}$-Neu5Ac was extracted from nanoparticles by dissolving 1 mg of nanoparticles in 100 μL of DMSO followed by centrifugation at 14 000 rpm for 10 min. 25 μL of supernatant or standard was assayed with HPLC, and the concentration P-3F$_{ax}$-Neu5Ac and loading efficiency was calculated as percentage of loaded amount of P-3F$_{ax}$-Neu5Ac relative to the total amount of nanoparticles. The loading efficiency of all prepared batches was about 1%.

Cell Culture. Mouse B16−F10 melanoma cells (CRL-6475, ATCC) were cultured in minimum essential medium (MEM) (Gibco, Invitrogen, Carlsbad, CA) containing 5% fetal bovine serum (FBS) (Greiner Bio-one, Frickenhausen, Germany), 1% MEM nonessential amino acids (Gibco), 0.15% sodium bicarbonate (Gibco), 1 mM sodium pyruvate (Gibco), 1.5% MEM vitamins (Gibco) and 0.5% antibiotic-antimycotic solution (50 U/mL penicillin, 50 μg/mL streptomycin and 125 ng/mL amphotericin B) (PAA, Pasching, Austria) in a humidified CO_2 incubator at 37 °C. 9464D neuroblastoma cells (kindly provided by R. Orentas, Department of Pediatrics, Medical College of Wisconsin, WI, USA) were cultured in Dulbecco's modified Eagle's medium (Glutamax, Gibco) containing 10% FBS, 1% nonessential amino acids, 20 μM 2-mercaptoethanol (Sigma-Aldrich) and 1% antibiotic-antimycotic solution.[61]

Extracellular Staining and Flow Cytometry. B16−F10 cells were incubated in suspension for 1 h with biotinylated MALII (5 μg/mL), SNA-I (1 μg/mL), PNA (5 μg/mL) or WGA (5 μg/mL) in carbo-free blocking solution containing 1 mM $CaCl^{2+}$ and 1 mM $MgCl^{2+}$ at 4 °C. MALII was used to detect α2,3-linked sialic acids, SNA-I for α2,6-linked sialic acids, PNA for terminal (β-)galactose/T antigen and WGA for detection of (poly)GlcNAc (chitobiose). Cells were washed in FACS buffer (1× PBS containing 1% FBS and 0.02% sodium azide) and cell-bound biotinylated lectins were conjugated for 10 min at 4 °C with 2 μg/mL streptavidin-phycoerythrin. Cells stained solely with streptavidin-phycoerythrin were used as background control. The percentage lectin binding was calculated by normalizing the fluorescence values from the bound lectins to the respective control. For detection of TRP-1 expression, B16−F10 or 9464D cells were stained with anti-TRP-1 or isotype control antibody for 15 min at 4 °C, washed and incubated 15 min with phycoerythrin conjugated

goat antimouse IgG antibody. Cells were washed with FACS buffer, stained with 7-AAD viability dye and resuspended in FACS buffer. Fluorescence was measured using a CyAn ADP flow cytometer or FACSCalibur flow cytometer (BD Biosciences, San Jose, CA) and quantified utilizing FlowJo software.

Nanoparticle Titration, Cellular Uptake and Binding. To determine the effective dose, B16−F10 cells were cultured for 3 days in medium containing 0−1 mg/mL P-3F$_{ax}$-Neu5Ac-loaded, P-3F$_{ax}$-Neu5Ac/A647-loaded or 0−2 mg/mL empty PLGA nanoparticles and stained with biotinylated lectins to assess the sialylation status. Lectin binding to empty PLGA nanoparticles-treated cells was used to normalize mean fluorescence intensities. To quantify cellular uptake of unmodified and antibody-conjugated P-3F$_{ax}$-Neu5Ac/A647- or DQ-BSA-loaded PLGA nanoparticles, B16−F10 cells or 9464D cells were cultured for 0−72 h in the presence of 1 mg/mL nanoparticles at 37 or 4 °C. Alternatively, B16−F10 cells were coincubated 20 min with 10 μg/mL anti-TRP-1 or isotype control antibody (which remained also present during the uptake experiment) or for 3 days with 23.1 μg/mL free P-3F$_{ax}$-Neu5Ac prior to the uptake experiment. Cells were thoroughly washed and fluorescent signal of ATTO 647 was measured directly by flow cytometry and quantified with FlowJo software. After washing, cells treated with DQ-BSA loaded PLGA nanoparticles were incubated 16 h before measurement to allow degradation of nanoparticles and DQ-BSA. To determine extracellular binding of antibody conjugated P-3F$_{ax}$-Neu5Ac/A647 nanoparticles, B16−F10 cells were incubated for 15 min at 4 °C, thoroughly washed and analyzed by flow cytometry.

Confocal Microscopy. To determine uptake or binding of unmodified or antibody-conjugated P-3F$_{ax}$-Neu5Ac/A647-loaded PLGA nanoparticles, B16−F10 cells were seeded on glass slides and allowed to attach for 1 h followed by incubation with 0.5 mg/mL nanoparticles for 1, 2, or 24 h at 37 °C. Next, cells were washed extensively with 1× PBS to remove free nanoparticles, fixated for 10 min with 2% paraformaldehyde on ice and blocked 30 min with carbo-free blocking solution. Additionally, cell membranes were stained by incubating the fixated cells 45 min with 10 μg/mL biotinylated WGA in carbo-free blocking solution at 4 °C followed by 20 min incubation with 5 μg/mL NeutrAvidin-Texas Red. Nuclei were stained by incubating the cells 10 min with DAPI. Samples were washed, mounted with Mowiol and images were acquired using an Olympus FV1000 confocal laser scanning microscope (Olympus, Tokyo, Japan). Images were processed and orthogonal projections were generated using ImageJ (NIH, Bethesda, MD).

Nanoparticle Kinetics and Stability. To compare the efficacy of nanoparticle encapsulated P-3F$_{ax}$-Neu5Ac *versus* soluble P-3F$_{ax}$-Neu5Ac, B16−F10 cells were cultured for 10 days in medium containing 1 mg/mL P-3F$_{ax}$-Neu5Ac nanoparticles or equal amounts of soluble inhibitor (23.1 μg/mL). Empty PLGA nanoparticles were used as control and medium was not replenished during the experiment. At various time points, cells were collected and stained with biotinylated MALII, SNA-I and PNA to assess cell surface expression of sialic acids with flow cytometry. Recovery speed of sialic acid expression was determined after incubating B16−F10 cells 3 days with 1 mg/mL antibody-conjugated P-3F$_{ax}$-Neu5Ac nanoparticles, the same amount of soluble inhibitor (23.1 μg/mL) or empty PLGA nanoparticles. After extensive washing, cells were kept in culture for 6 days and sialylation was measured every day by flow cytometry using MALII, SNA-I and PNA lectins.

To determine stability of unmodified or PEGylated P-3F$_{ax}$-Neu5Ac nanoparticles, 1 mg/mL nanoparticles or an equal amount of soluble P-3F$_{ax}$-Neu5Ac (23.1 μg/mL) were incubated for 0−10 days at 37 °C. At several time points, supernatant and nanoparticle fractions were collected by centrifugation 14 000 rpm for 10 min. B16−F10 cells were cultured for 3 days with the collected fractions and 0−17.6 μg/mL fresh P-3F$_{ax}$-Neu5Ac. Expression of α2,3-linked sialic acids was measured by flow cytometry using MALII lectin.

Pulmonary Metastasis Model and Histology. B16−F10 cells were treated 3 days with PBS, 23,1 μg/mL P-3F$_{ax}$-Neu5Ac or for 45 min with 150mU. Cells were thoroughly washed and collected in 1× PBS. 200 μL PBS containing either 0.2 × 10^6 or 0.5 × 10^6 pretreated B16−10 cells were injected into the tail vein of mice. For *in vivo* targeting, 20 mg/kg (0.4 mg in 50 μL PBS) anti-TRP-1 or isotype antibody-conjugated P-3F$_{ax}$-Neu5Ac nanoparticles were injected intravenously, and 1 h later, 0.5 × 10^6 B16−10 cells were injected intravenously. Sixteen hours following injection with B16−F10 cells a second dose 20 mg/kg (0.4 mg in 50 μL PBS) anti-TRP-1 or isotype antibody-conjugated P-3F$_{ax}$-Neu5Ac nanoparticles was injected intravenously. Fourteen days post injection, mice were euthanized and lungs were collected. The treatment schedule is depicted in Figure 6a. The lungs were rinsed with PBS and fixed overnight in 1× Fekete's solution (distilled water containing 70% absolute ethanol, 10% 37% formaldehyde solution and 4.5% glacial acetic acid) at room temperature. Pulmonary lesions, melanotic (black) and amelanotic (gray/white), were counted using a stereo microscope, and representative images were taken. For histology, lungs were fixed in 4% phosphate-buffered formaldehyde, embedded in paraffin, sectioned and stained with hematoxylin and eosin.

Statistical Analysis. Statistical significance between two groups was determined by an unpaired *t* test and for multiple comparisons one-way analysis of variance (ANOVA), followed by Bonferroni's correction performed using Prism 5.03 (GraphPad Software, Inc., La Jolla, CA). *P*-values < 0.05 were considered significant ($p < 0.05$ *, $p < 0.01$ **, $p < 0.001$ ***).

Conflict of Interest: The authors declare no competing financial interest.

Acknowledgment. We thank M. Verdoes for scientific discussions and J. Mooren for excellent caretaking of the animals. This work was supported by a Radboud University Medical Center Ph.D. Grant awarded to C. Büll, a grant from the Scientific Research (NWO) Rubicon program awarded to T. J. Boltje, and a grant from the Dutch Cancer Society (2009−4402). C. G. Figdor is recipient of an ERC Advanced Grant (PATHFINDER-269019) and an NWO Spinoza Award.

Supporting Information Available: Figure S1. Desialylation abrogates metastases formation; Table S1. Characteristics of P-3Fax-Neu5Ac and P-3Fax-Neu5Ac/A647 nanoparticles; Figure S2. Blockage of sialylation with P-3Fax-Neu5Ac NPs *versus* soluble P-3Fax-Neu5Ac; Figure S3. (P-3Fax-Neu5Ac) PLGA NPs are nontoxic and do not affect cellular glycosylation; Figure S4. Co-delivery of P-3Fax-Neu5Ac and ATTO 647 to B16−F10 cells using NPs; Figure S5. Uptake of P-3Fax-Neu5Ac/A647 NPs in B16−F10 cells; Figure S6. Blockage kinetics of P-3Fax-Neu5Ac NPs *versus* soluble P-3Fax-Neu5Ac. Figure S7. Expression of TRP-1 on B16−F10 cells and 9464 cells and uptake of αTRP-1-targeting; Figure S8. Stability of unmodified or PEGylated P-3FaxNeu5Ac NPs; Figure S9. Expression of TRP-1 and α-TRP-1 NPs uptake following P-3FaxNeu5Ac treatment. This material is available free of charge *via* the Internet at http://pubs.acs.org.

REFERENCES AND NOTES

1. Sakuma, K.; Aoki, M.; Kannagi, R. Transcription Factors c-Myc and CDX2Mediate E-Selectin Ligand Expression in Colon Cancer Cells Undergoing EGF/bFGF-Induced Epithelial-Mesenchymal Transition. *Proc. Natl. Acad. Sci. U. S. A.* **2012**, *109*, 7776–7781.
2. Matsumoto, A.; Cabral, H.; Sato, N.; Kataoka, K.; Miyahara, Y. Assessment of Tumor Metastasis by the Direct Determination of Cell-Membrane Sialic Acid Expression. *Angew. Chem., Int. Ed. Engl.* **2010**, *49*, 5494–5497.
3. Chen, J. Y.; Tang, Y. A.; Huang, S. M.; Juan, H. F.; Wu, L. W.; Sun, Y. C.; Wang, S. C.; Wu, K. W.; Balraj, G.; Chang, T. T.; *et al.* A Novel Sialyltransferase Inhibitor Suppresses FAK/Paxillin Signaling and Cancer Angiogenesis and Metastasis Pathways. *Cancer Res.* **2011**, *71*, 473–483.
4. Julien, S.; Ivetic, A.; Grigoriadis, A.; QiZe, D.; Burford, B.; Sproviero, D.; Picco, G.; Gillett, C.; Papp, S. L.; Schaffer, L.; *et al.* Selectin Ligand Sialyl-Lewis X Antigen Drives Metastasis of Hormone-Dependent Breast Cancers. *Cancer Res.* **2011**, *71*, 7683–7693.
5. Perez-Garay, M.; Arteta, B.; Pages, L.; de Llorens, R.; de Bolos, C.; Vidal-Vanaclocha, F.; Peracaula, R.

Alpha2,3-Sialyltransferase ST3Gal III Modulates Pancreatic Cancer Cell Motility and Adhesion *In Vitro* And Enhances its Metastatic Potential *In Vivo*. *PLoS One* **2010**, 10.1371/journal.pone.0012524.
6. Varki, A.; Kannagi, R.; Toole, B. P. Glycosylation Changes in Cancer. In *Essentials of Glycobiology*, 2nd ed.; Varki, A., Cummings, R. D., Esko, J. D., Freeze, H. H., Stanley, P., Bertozzi, C. R., Hart, G. W., Etzler, M. E., Eds.; Cold Spring Harbor Laboratory Press: Cold Spring Harbor, NY, 2009.
7. Paszek, M. J.; DuFort, C. C.; Rossier, O.; Bainer, R.; Mouw, J. K.; Godula, K.; Hudak, J. E.; Lakins, J. N.; Wijekoon, A. C.; Cassereau, L.; *et al.* The Cancer Glycocalyx Mechanically Primes Integrin-Mediated Growth and Survival. *Nature* **2014**, *511*, 319–325.
8. Plaks, V.; Koopman, C. D.; Werb, Z. Cancer. Circulating Tumor Cells. *Science* **2013**, *341*, 1186–1188.
9. Chambers, A. F.; Groom, A. C.; MacDonald, I. C. Dissemination and Growth of Cancer Cells in Metastatic Sites. *Nat. Rev. Cancer* **2002**, *2*, 563–572.
10. Fidler, I. J. The Pathogenesis of Cancer Metastasis: The 'Seed and Soil' Hypothesis Revisited. *Nat. Rev. Cancer* **2003**, *3*, 453–458.
11. Reymond, N.; d'Agua, B. B.; Ridley, A. J. Crossing the Endothelial Barrier During Metastasis. *Nat. Rev. Cancer* **2013**, *13*, 858–870.
12. Gay, L. J.; Felding-Habermann, B. Contribution of Platelets to Tumour Metastasis. *Nat. Rev. Cancer* **2011**, *11*, 123–134.
13. Kannagi, R.; Izawa, M.; Koike, T.; Miyazaki, K.; Kimura, N. Carbohydrate-Mediated Cell Adhesion in Cancer Metastasis and Angiogenesis. *Cancer Sci.* **2004**, *95*, 377–384.
14. Schultz, M. J.; Swindall, A. F.; Bellis, S. L. Regulation of the Metastatic Cell Phenotype by Sialylated Glycans. *Cancer Metastasis Rev.* **2012**, *31*, 501–518.
15. Büll, C.; Stoel, M. A.; den Brok, M. H.; Adema, G. J. Sialic Acids Sweeten a Tumor's Life. *Cancer Res.* **2014**, *74*, 3199–3204.
16. Varki, A.; Schauer, R. Sialic Acids. In *Essentials of Glycobiology*, 2nd ed.; Varki, A., Cummings, R. D., Esko, J. D., Freeze, H. H., Stanley, P., Bertozzi, C. R., Hart, G. W., Etzler, M. E., Eds.; Cold Spring Harbor Laboratory Press: Cold Spring Harbor, NY, 2009.
17. Swindall, A. F.; Londono-Joshi, A. I.; Schultz, M. J.; Fineberg, N.; Buchsbaum, D. J.; Bellis, S. L. ST6Gal-I Protein Expression is Upregulated in Human Epithelial Tumors and Correlates with Stem Cell Markers in Normal Tissues and Colon Cancer Cell Lines. *Cancer Res.* **2013**, *73*, 2368–2378.
18. Harduin-Lepers, A.; Krzewinski-Recchi, M. A.; Colomb, F.; Foulquier, F.; Groux-Degroote, S.; Delannoy, P. Sialyltransferases Functions in Cancers. *Front. Biosci., Elite Ed.* **2012**, *4*, 499–515.
19. Häuselmann, I.; Borsig, L. Altered Tumor-Cell Glycosylation Promotes Metastasis. *Front. Oncol.* **2014**, *4*, 28.
20. Amano, M.; Eriksson, H.; Manning, J. C.; Detjen, K. M.; Andre, S.; Nishimura, S.; Lehtio, J.; Gabius, H. J. Tumour Suppressor p16(INK4a)—Anoikis-Favouring Decrease in N/O-Glycan/Cell Surface Sialylation by Down-Regulation of Enzymes in Sialic Acid Biosynthesis in Tandem in a Pancreatic Carcinoma Model. *FEBS J.* **2012**, *279*, 4062–4680.
21. Büll, C.; den Brok, M. H.; Adema, G. J. Sweet Escape: Sialic Acids in Tumor Immune Evasion. *Biochim. Biophys. Acta, Rev. Cancer* **2014**, *1864*, 238–246.
22. Bos, P. D.; Zhang, X. H.; Nadal, C.; Shu, W.; Gomis, R. R.; Nguyen, D. X.; Minn, A. J.; van de Vijver, M. J.; Gerald, W. L.; Foekens, J. A.; *et al.* Genes that Mediate Breast Cancer Metastasis to the Brain. *Nature* **2009**, *459*, 1005–1009.
23. Uemura, T.; Shiozaki, K.; Yamaguchi, K.; Miyazaki, S.; Satomi, S.; Kato, K.; Sakuraba, H.; Miyagi, T. Contribution of Sialidase Neu1 to Suppression of Metastasis of Human Colon Cancer Cells through Desialylation of Integrin Beta 4. *Oncogene* **2009**, *28*, 1218–1229.
24. Sawada, M.; Moriya, S.; Saito, S.; Shineha, R.; Satomi, S.; Yamori, T.; Tsuruo, T.; Kannagi, R.; Miyagi, T. Reduced Sialidase Expression in Highly Metastatic Variants of Mouse Colon Adenocarcinoma 26 and Retardation of their Metastatic Ability by Sialidase Overexpression. *Int. J. Cancer* **2002**, *97*, 180–185.
25. Kato, T.; Wang, Y.; Yamaguchi, K.; Milner, C. M.; Shineha, R.; Satomi, S.; Miyagi, T. Overexpression of Lysosomal-Type Sialidase Leads to Suppression of Metastasis Associated with Reversion of Malignant Phenotype in Murine B16 Melanoma Cells. *Int. J. Cancer* **2001**, *92*, 797–804.
26. Gasic, G. J.; Gasic, T. B.; Stewart, C. C. Antimetastatic Effects Associated with Platelet Reduction. *Proc. Natl. Acad. Sci. U. S. A.* **1968**, *61*, 46–52.
27. Weiss, L.; Glaves, D.; Waite, D. A. The Influence of Host Immunity on the Arrest of Circulating Cancer Cells, and its Modification by Neuraminidase. *Int. J. Cancer* **1974**, *13*, 850–862.
28. Rillahan, C. D.; Antonopoulos, A.; Lefort, C. T.; Sonon, R.; Azadi, P.; Ley, K.; Dell, A.; Haslam, S. M.; Paulson, J. C. Global Metabolic Inhibitors of Sialyl- and Fucosyltransferases Remodel the Glycome. *Nat. Chem. Biol.* **2012**, *8*, 661–668.
29. Büll, C.; Boltje, T. J.; Wassink, M.; de Graaf, A. M.; van Delft, F. L.; den Brok, M. H.; Adema, G. J. Targeting Aberrant Sialylation in Cancer Cells Using a Fluorinated Sialic Acid Analog Impairs Adhesion, Migration, and *In Vivo* Tumor Growth. *Mol. Cancer Ther.* **2013**, *12*, 1935–1946.
30. Danhier, F.; Ansorena, E.; Silva, J. M.; Coco, R.; Le Breton, A.; Preat, V. PLGA-Based Nanoparticles: An Overview of Biomedical Applications. *J. Controlled Release* **2012**, *161*, 505–522.
31. Cruz, L. J.; Tacken, P. J.; Fokkink, R.; Joosten, B.; Stuart, M. C.; Albericio, F.; Torensma, R.; Figdor, C. G. Targeted PLGA Nano- But not Microparticles Specifically Deliver Antigen to Human Dendritic Cells *via* Dc-Sign *In Vitro*. *J. Controlled Release* **2010**, *144*, 118–126.
32. Tacken, P. J.; Zeelenberg, I. S.; Cruz, L. J.; van Hout-Kuijer, M. A.; van de Glind, G.; Fokkink, R. G.; Lambeck, A. J.; Figdor, C. G. Targeted Delivery of TLR Ligands to Human and Mouse Dendritic Cells Strongly Enhances Adjuvanticity. *Blood* **2011**, *118*, 6836–6844.
33. Giannotti, M. I.; Esteban, O.; Oliva, M.; Garcia-Parajo, M. F.; Sanz, F. PH-Responsive Polysaccharide-Based Polyelectrolyte Complexes as Nanocarriers for Lysosomal Delivery of Therapeutic Proteins. *Biomacromolecules* **2011**, *12*, 2524–2533.
34. Cartiera, M. S.; Johnson, K. M.; Rajendran, V.; Caplan, M. J.; Saltzman, W. M. The Uptake and Intracellular Fate of PLGA Nanoparticles in Epithelial Cells. *Biomaterials* **2009**, *30*, 2790–2798.
35. Raposo, G.; Marks, M. S. Melanosomes—Dark Organelles Enlighten Endosomal Membrane Transport. *Nat. Rev. Mol. Cell Biol.* **2007**, *8*, 786–797.
36. Setty, S. R.; Tenza, D.; Truschel, S. T.; Chou, E.; Sviderskaya, E. V.; Theos, A. C.; Lamoreux, M. L.; Di Pietro, S. M.; Starcevic, M.; Bennett, D. C.; *et al.* BLOC-1 is Required for Cargo-Specific Sorting from Vacuolar Early Endosomes Toward Lysosome-Related Organelles. *Mol. Biol. Cell* **2007**, *18*, 768–780.
37. Ribic, C. M.; Sargent, D. J.; Moore, M. J.; Thibodeau, S. N.; French, A. J.; Goldberg, R. M.; Hamilton, S. R.; Laurent-Puig, P.; Gryfe, R.; Shepherd, L. E.; *et al.* Tumor Microsatellite-Instability Status as a Predictor of Benefit from Fluorouracil-Based Adjuvant Chemotherapy for Colon Cancer. *N. Engl. J. Med.* **2003**, *349*, 247–257.
38. Overwijk, W. W.; Restifo, N. P. B16 as a Mouse Model for Human Melanoma. In *Current Protocols in Immunology*; Wiley: New York, 2001; Chapter 20, Unit 20-1.
39. Fuster, M. M.; Esko, J. D. The Sweet and Sour of Cancer: Glycans as Novel Therapeutic Targets. *Nat. Rev. Cancer* **2005**, *5*, 526–542.
40. Seales, E. C.; Jurado, G. A.; Brunson, B. A.; Wakefield, J. K.; Frost, A. R.; Bellis, S. L. Hypersialylation of Beta1 Integrins, Observed in Colon Adenocarcinoma, May Contribute to Cancer Progression by Up-Regulating Cell Motility. *Cancer Res.* **2005**, *65*, 4645–4652.
41. Zhuo, Y.; Bellis, S. L. Emerging Role of Alpha2,6-Sialic Acid as a Negative Regulator of Galectin Binding and Function. *J. Biol. Chem.* **2011**, *286*, 5935–5941.
42. Macauley, M. S.; Arlian, B. M.; Rillahan, C. D.; Pang, P. C.; Bortell, N.; Marcondes, M. C.; Haslam, S. M.; Dell, A.; Paulson,

J. C. Systemic Blockade of Sialylation in Mice With a Global Inhibitor of Sialyltransferases. *J. Biol. Chem.* **2014**, *289*, 35149–35158.
43. Galeano, B.; Klootwijk, R.; Manoli, I.; Sun, M.; Ciccone, C.; Darvish, D.; Starost, M. F.; Zerfas, P. M.; Hoffmann, V. J.; Hoogstraten-Miller, S.; *et al.* Mutation in the Key Enzyme of Sialic Acid Biosynthesis Causes Severe Glomerular Proteinuria and Is Rescued by N-Acetylmannosamine. *J. Clin. Invest.* **2007**, *117*, 1585–1594.
44. Negroiu, G.; Branza-Nichita, N.; Petrescu, A. J.; Dwek, R. A.; Petrescu, S. M. Protein Specific N-Glycosylation of Tyrosinase and Tyrosinase-Related Protein-1 in B16 Mouse Melanoma Cells. *Biochem. J.* **1999**, *344* (Pt 3), 659–665.
45. Leunissen, E. H.; Nair, A. V.; Büll, C.; Lefeber, D. J.; van Delft, F. L.; Bindels, R. J.; Hoenderop, J. G. The Epithelial Calcium Channel TRPV5 is Regulated Differentially by Klotho and Sialidase. *J. Biol. Chem.* **2013**, *288*, 29238–29246.
46. Kim, M. Y.; Oskarsson, T.; Acharyya, S.; Nguyen, D. X.; Zhang, X. H.; Norton, L.; Massague, J. Tumor Self-Seeding by Circulating Cancer Cells. *Cell* **2009**, *139*, 1315–1326.
47. Leung, C. T.; Brugge, J. S. Tumor Self-Seeding: Bidirectional Flow of Tumor Cells. *Cell* **2009**, *139*, 1226–1228.
48. Alonso, D. F.; Ripoll, G. V.; Garona, J.; Iannucci, N. B.; Gomez, D. E. Metastasis: Recent Discoveries and Novel Perioperative Treatment Strategies with Particular Interest in the Hemostatic Compound Desmopressin. *Curr. Pharm. Biotechnol.* **2011**, *12*, 1974–1980.
49. van der Bij, G. J.; Oosterling, S. J.; Beelen, R. H. J.; Meijer, S.; Coffey, J. C.; van Egmond, M. The Perioperative Period is an Underutilized Window of Therapeutic Opportunity in Patients With Colorectal Cancer. *Ann. Surg.* **2009**, *249*, 727–734.
50. Daenen, L. G.; Roodhart, J. M.; van Amersfoort, M.; Dehnad, M.; Roessingh, W.; Ulfman, L. H.; Derksen, P. W.; Voest, E. E. Chemotherapy Enhances Metastasis Formation *via* VEGFR-1-Expressing Endothelial Cells. *Cancer Res.* **2011**, *71*, 6976–6985.
51. Sofia Vala, I.; Martins, L. R.; Imaizumi, N.; Nunes, R. J.; Rino, J.; Kuonen, F.; Carvalho, L. M.; Ruegg, C.; Grillo, I. M.; Barata, J. T.; *et al.* Low Doses of Ionizing Radiation Promote Tumor Growth and Metastasis by Enhancing Angiogenesis. *PLoS One* **2010**, *5*, e11222.
52. Yoon, H. J.; Kozminsky, M.; Nagrath, S. Emerging Role of Nanomaterials in Circulating Tumor Cell Isolation and Analysis. *ACS Nano* **2014**, *8*, 1995–2017.
53. Smerage, J. B.; Barlow, W. E.; Hortobagyi, G. N.; Winer, E. P.; Leyland-Jones, B.; Srkalovic, G.; Tejwani, S.; Schott, A. F.; O'Rourke, M. A.; Lew, D. L.; *et al.* Circulating Tumor Cells and Response to Chemotherapy in Metastatic Breast Cancer: SWOG S0500. *J. Clin. Oncol.* **2014**, *32*, 3483–3489.
54. Boross, P.; Jansen, J. H.; van Tetering, G.; Nederend, M.; Brandsma, A.; Meyer, S.; Torfs, E.; van den Ham, H. J.; Meulenbroek, L.; de Haij, S.; *et al.* Anti-Tumor Activity of Human IgG1 Anti-gp75 TA99 mAb against B16F10 Melanoma in Human Fc gamma RI Transgenic Mice. *Immunol. Lett.* **2014**, *160*, 151–157.
55. Albanesi, M.; Mancardi, D. A.; Macdonald, L. E.; Iannascoli, B.; Zitvogel, L.; Murphy, A. J.; Daeron, M.; Leusen, J. H.; Bruhns, P. Cutting Edge: Fc Gamma RIII (CD16) and Fc GammaRI (CD64) Are Responsible for Anti-Glycoprotein 75 Monoclonal Antibody TA99 Therapy for Experimental Metastatic B16 Melanoma. *J. Immunol.* **2012**, *189*, 5513–5517.
56. Bevaart, L.; Jansen, M. J.; van Vugt, M. J.; Verbeek, J. S.; van de Winkel, J. G.; Leusen, J. H. The High-Affinity IgG Receptor, Fc Gamma RI, Plays a Central Role in Antibody Therapy of Experimental Melanoma. *Cancer Res.* **2006**, *66*, 1261–1264.
57. Watabe, H.; Valencia, J. C.; Yasumoto, K.; Kushimoto, T.; Ando, H.; Muller, J.; Vieira, W. D.; Mizoguchi, M.; Appella, E.; Hearing, V. J. Regulation of Tyrosinase Processing and Trafficking by Organellar pH and by Proteasome Activity. *J. Biol. Chem.* **2004**, *279*, 7971–7981.
58. Lavik, E.; von Recum, H. The Role of Nanomaterials in Translational Medicine. *ACS Nano* **2011**, *5*, 3419–3424.
59. Karra, N.; Nassar, T.; Ripin, A. N.; Schwob, O.; Borlak, J.; Benita, S. Antibody Conjugated PLGA Nanoparticles for Targeted Delivery of Paclitaxel Palmitate: Efficacy and Biofate in a Lung Cancer Mouse Model. *Small* **2013**, *9*, 4221–4236.
60. Jain, A. K.; Das, M.; Swarnakar, N. K.; Jain, S. Engineered PLGA Nanoparticles: An Emerging Delivery Tool in Cancer Therapeutics. *Crit. Rev. Ther. Drug Carrier Syst.* **2011**, *28*, 1–45.
61. Kroesen, M.; Nierkens, S.; Ansems, M.; Wassink, M.; Orentas, R. J.; Boon, L.; den Brok, M. H.; Hoogerbrugge, P. M.; Adema, G. J. A Transplantable TH-MYCN Transgenic Tumor Model In C57BL/6 Mice for Preclinical Immunological Studies in Neuroblastoma. *Int. J. Cancer* **2014**, *134*, 1335–45.